

Cyclic Azobenzene-Containing Side-Chain Liquid Crystalline Polymers: Synthesis and Topological Effect on Mesophase Transition, Order, and Photoinduced Birefringence

Dehui Han,[†] Xia Tong,[†] Yi Zhao,[†] Tigran Galstian,[‡] and Yue Zhao*,[†]

[†]Département de chimie, Université de Sherbrooke, Sherbrooke, Québec, Canada J1K 2R1, and

[‡]Centre d'Optique, Photonique et Lasers, Département de Physique, Université Laval, 2375 Rue de la Terrasse, Québec, Canada G1V 0A6

Received February 3, 2010; Revised Manuscript Received March 12, 2010

ABSTRACT: A cyclic side-chain liquid crystalline polymer (SCLCP) bearing azobenzene mesogens, namely, poly{6-[4-(4-methoxyphenylazo)phenoxy]hexyl methacrylate} (PAzoMA), was successfully synthesized by using “click” cyclization of the linear polymer precursor with alkyne and azido end groups. Samples of cyclic-PAzoMA of various molecular weights were prepared, characterized, and studied in comparison with their linear counterparts. The results show that the topological constraint arising from the tortuosity of the ring structure and the absence of chain ends in cyclic-SCLCPs affects profoundly the liquid crystalline (LC) phase transitions (temperature, enthalpy, and entropy) of mesogenic side groups and that this topological effect is more prominent for smaller SCLCP rings. Moreover, the photoinduced anisotropy in films as a result of the trans–cis photoisomerization of azobenzene mesogens was investigated, and cyclic-PAzoMA was found to behave differently from linear-PAzoMA. On the one hand, the cyclic polymer exhibits a nonmonotonic rise and erasure of birefringence upon linearly and circularly polarized excitation (488 nm), respectively, in contrast with the linear polymer displaying monotonic changes. On the other hand, unlike the linear polymer, the photoinduced orientation of azobenzene mesogens in cyclic-PAzoMA cannot be enhanced upon annealing in the nematic phase. All these manifestations of the topological constraint suggest that cyclization offers a new way to change the coupling between mesogenic side groups and chain backbone of SCLCPs, and their interplay under the additional topological effect may generate new behaviors that are of interest to be explored.

Introduction

The importance of cyclic polymers in biological and macromolecular sciences has long been recognized.^{1–3} Compared with linear polymers, there are relatively few reports on cyclic polymers, and the number of cyclic polymers studied is limited as well, partly due to the more demanding synthetic procedures. In recent years, there has been a growing interest in cyclic polymers thanks to the development of a number of efficient synthetic methods that make their preparation more accessible.^{4–11} Of them, the “click” cyclization of α -alkynyl- ω -azido heterodifunctional linear polymers under high dilution is particularly attractive, since it can be applied to many polymers synthesized by using atom transfer radical polymerization (ATRP).^{6–9} Cyclic polymers display distinct topological features; the tortuosity of the chain ring structure and the absence of chain ends could make them to behave differently from their linear counterparts both in solution and in the melt.^{1–12} In solution, the most investigated properties of cyclic polymers are the hydrodynamic volume, radius of gyration, and viscosity. Noticeably, a recent study of Xu et al. found different thermal phase transition behaviors of cyclic poly(*N*-isopropylacrylamide) (PNIPAM) in aqueous solution as compared to the linear polymer.⁷ In the bulk, in addition to the viscosity and thermostability, the glass transition temperature (T_g) (e.g., for cyclic polystyrene)¹³ and the melting temperature (T_m) (mainly for cyclic poly(ethylene oxide))¹⁴ have also been studied. In the case of liquid crystalline polymers (LCPs), Percec et al. studied cyclic LC oligomers (with up to 4–5 mesogenic units

on the ring)¹⁵ and polymers bearing these cyclic oligomers as side groups or on the main chain.¹⁶ Overall, however, cyclic functional or stimuli-responsive polymers have not been much explored until now, and their full potential in the development of new functional materials remains to be unveiled.

This paper reports the synthesis and characterization of, to our knowledge, the first cyclic side-chain liquid crystalline polymer (cyclic-SCLCP) with pendant azobenzene mesogenic groups. The successful synthesis of cyclic-SCLCP was achieved by using the aforementioned “click” cyclization method. We anticipated that the topological constraint of cyclic polymers could affect the LC phase transitions of mesogenic side groups. By having azobenzene mesogens, the effect of the cyclic structure on the photoinduced anisotropy upon trans–cis photoisomerization could also be investigated. As reported in this paper, the results of our comparative study with cyclic-SCLCP and their linear precursors (linear-SCLCP) revealed profound, and sometimes surprising, topological effects on the mesophase transitions and the photoinduced anisotropy.

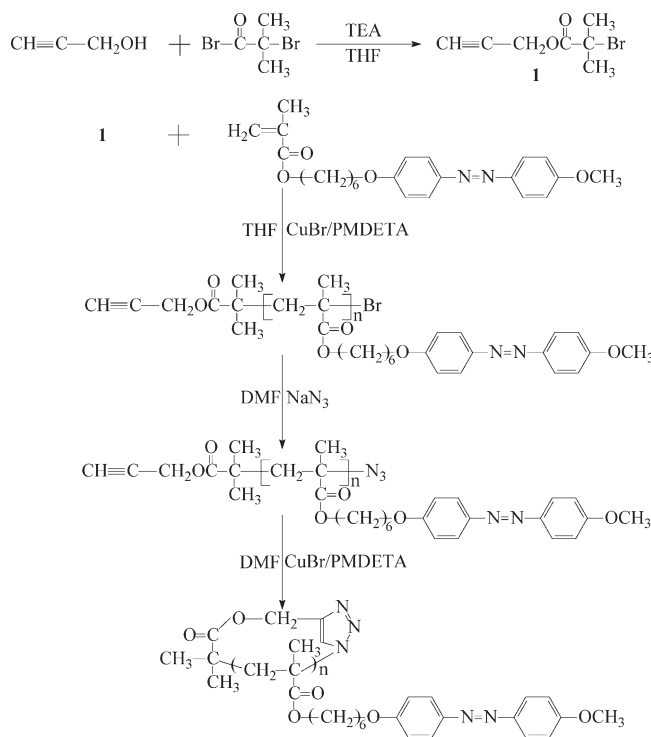
Experimental Section

1. Polymer Synthesis. The synthetic route to the cyclic azobenzene-containing SCLCP is depicted in Scheme 1. More details are given below.

Materials. Prior to use, tetrahydrofuran (THF, 99%) was refluxed with sodium and a small amount of benzophenone and distilled, triethylamine (TEA) (Aldrich, $\geq 99\%$) was refluxed with *p*-toluenesulfonyl chloride (Fluka, $\geq 99\%$) and distilled, and *N*,*N*-dimethylformamide (DMF, 99.8%) was dried with anhydrous

*Corresponding author. E-mail: yue.zhao@usherbrooke.ca.

Scheme 1. Synthetic Route to Cyclic Azobenzene-Containing Side-Chain Liquid Crystalline Polymers



magnesium sulfate and distilled under reduced pressure. Dichloromethane (DCM) was distilled from CaH₂. Copper(I) bromide (CuBr, 99.999%), α-bromoisobutyryl bromide (98%), *N,N,N',N'*-pentamethyldiethylenetriamine (PMDETA, 99%), and propargyl alcohol (99%) were purchased from Aldrich and used directly. The monomer with an azobenzene group, 6-[4-(4-methoxyphenylazo)phenoxy]hexyl methacrylate (AzOMA), was synthesized by using a literature method.¹⁷

Synthesis of ATRP Initiator: Propargyl 2-Bromoisobutyrate. Into a 250 mL round-bottom flask with a magnetic stirrer, propargyl alcohol (7.0 g, 130 mmol), TEA (17.5 mL, 130 mmol), and CH₂Cl₂ (100 mL) were added. After the mixture was cooled to 0 °C, α-bromoisobutyryl bromide (28.8 g, 130 mmol) was added dropwise over a period of 30 min. The reaction mixture was then brought back to room temperature and stirred for 24 h. The salt formed was removed by filtration, and the filtrate was washed with NaCl solution several times. The organic phase was dried over MgSO₄. After the removal of solvent under reduced pressure, the colorless propargyl 2-bromoisobutyrate was obtained by distillation under reduced pressure. ¹H NMR (300 MHz, CDCl₃, δ (TMS, ppm): 4.80 (2H, COOCH₂); 2.50 (1H, COOCH₂C≡CH); 1.96 (6H, C(CH₃)₂).

Synthesis of Linear Polymer Precursor (Linear-PAzoMA-N₃). Propargyl 2-bromoisobutyrate (0.01 g, 0.05 mmol), CuBr (7.06 mg, 0.05 mmol), AzOMA (1.5 g, 3.8 mmol), PMDETA (8.50 mg, 0.05 mmol), and THF (4.0 mL) were added successively into a 10 mL flask. The reaction mixture was degassed by three pump-thaw cycles, backfilled with N₂, and placed in an oil bath thermostated at 70 °C for 1.5 h. It was then diluted with THF and passed through a column of neutral alumina to remove the metal salt. After precipitation by adding the polymer solution of THF into methanol, the yellow polymer PAzoMA-Br was collected by filtration and then dried under vacuum overnight (0.63 g, yield 42%). Afterward, azide group-ended polymer was obtained as follows. PAzoMA-Br (0.50 g, 0.04 mmol), NaN₃ (0.023 g, 0.36 mmol), and DMF (5 mL) were added into a 10 mL round-bottom flask with a magnetic stirrer, and the reaction mixture was stirred for 24 h at room temperature. After purification by precipitation of the polymer solution into methanol

twice, the linear SCLCP precursor, linear PAzoMA-N₃, was collected (yellow solid, 0.43 g, yield 86%). ¹H NMR (600 MHz, δ ppm, CDCl₃): 7.83 (b, 4H, *o*-Ar H to −N=N−), 6.94 (b, 4H, *m*-Ar H to −N=N−), 4.60 (b, 2H, COOCH₂C≡CH), 3.95 (b, 4H, OCH₂), 3.84 (b, 3H, OCH₃), 1.96 (b, 6H, OOC(CH₃)₂), 1.2–2.0 (b, 10H, OCH₂CH₂CH₂CH₂CH₂O and main chain CH₂), 0.8–1.1 (b, 3H, main chain CH₃).

Synthesis of Cyclic Side-Chain Liquid Crystalline Polymer (Cyclic-PAzoMA). 160 mL of DMF was added into a 250 mL three-necked round-bottom flask, followed by three freeze-pump-thaw cycles for degassing. CuBr (205.6 mg, 1.4 mmol) and PMDETA (247.8 mg, 1.4 mmol) were then charged into the flask under protection of N₂ flow. Linear-PAzoMA-N₃ (0.10 g, 7.14 × 10⁻³ mmol) was dissolved in DMF (40 mL), and the solution was thoroughly deoxygenated by bubbling with N₂ for 1 h. Using a pressure-equalizing addition funnel, the polymer solution was added into the CuBr/PMDETA reaction mixture at 100 °C very slowly, over 24 h. After the addition of polymer solution was completed, the reaction was allowed to proceed for another period of 24 h. Afterward, DCM was used to extract the polymer after cooling the reaction mixture to room temperature. The organic phase was washed several times with saturated NaHSO₄ solution, dried over MgSO₄, and concentrated with a rotary evaporator. The resulting cyclic polymer, cyclic-PAzoMA, was then purified by precipitation in methanol (yellow solid, 0.072 g, 72% yield). ¹H NMR (600 MHz, δ ppm, CDCl₃): 7.83 (b, 4H, *o*-Ar H to −N=N−), 6.94 (b, 4H, *m*-Ar H to −N=N−), 5.20 (b, 2H, COOCH₂), 3.95 (b, 4H, OCH₂), 3.84 (b, 3H, OCH₃), 1.96 (b, 6H, OOC(CH₃)₂), 1.2–2.0 (b, 10H, OCH₂CH₂CH₂CH₂CH₂O and main chain CH₂), 0.8–1.1 (b, 3H, main chain CH₃).

2. Characterization. ¹H NMR spectra were recorded on a Bruker 600 MHz spectrometer using deuterated chloroform as solvent and tetramethylsilane as internal standard. The spectra were used to determine the number-average molecular weights (\overline{M}_n) of the linear polymer precursors. A Waters size exclusion chromatograph (SEC) instrument, equipped with a Waters 410 differential refractometer detector and a Waters 996 photodiode array detector, was also utilized to measure the number- and weight-average molecular weights (\overline{M}_n and \overline{M}_w) as well as the polydispersity index (PDI). The SEC measurements were conducted at 35 °C using one column (Waters Styragel HR4E, 7.8 mm × 300 mm, 5 μm beads), polystyrene (PS) standards for calibration, and THF as the eluent (flow rate: 1.0 mL min⁻¹). A TA Q200 differential scanning calorimeter (DSC) was used to investigate the phase transition behaviors, using indium as the calibration standard and a heating or cooling rate of 10 °C min⁻¹. The glass transition temperature (T_g) was measured as the midpoint of the change in heat capacity, while mesophase transition temperatures were taken as the maximum of the respective endothermic peak. Polarizing optical micrographs (POM) were obtained using a Leitz DMR-P microscope equipped with an Instec hot stage. UV-vis spectra were recorded with a Varian 50 Bio spectrophotometer, while Fourier transform infrared (FTIR) spectra were recorded on a Nicolet AVATAR 370 DTGS FTIR spectrometer.

3. Optical Measurements. Two types of optical measurements were performed in this study. On the one hand, the dynamic process of photoinduced birefringence in thick films (thickness ~10 μm) of cyclic- and linear-PAzoMA was monitored at room temperature by using a polarimetric optical setup described elsewhere.¹⁸ In essence, a polymer film, cast on a glass slide and preirradiated with a UV lamp to reach the photostationary *cis*-rich state, was placed between two crossed polarizers and exposed to a linearly polarized Ar⁺ ion laser beam ($\lambda = 488$ nm) with a small incident angle to the film normal. The polarization of the excitation beam was set at 45° with respect to the crossed polarizers, the excitation beam had a spot of about 2 mm in diameter, and its power was adjusted to be 42 mW. The photo-induced birefringence in the area hit by the Ar⁺ laser beam resulted

Table 1. Characteristics of Linear- and Cyclic Azobenzene-Containing Side-Chain Liquid Crystalline Polymers^a

sample	\overline{M}_n^b (g mol ⁻¹)	\overline{M}_n^c (g mol ⁻¹)	PDI ^c	T_g (°C)	T_{sn} (°C)	ΔH_{sn} (J g ⁻¹)	ΔS_{sn} (J g ⁻¹ K ⁻¹)	T_{ni} (°C)	ΔH_{ni} (J g ⁻¹)	ΔS_{ni} (J g ⁻¹ K ⁻¹)
linear-PAzoMA ₁₂	4750	6010	1.15	68.8	82.6	3.27	9.19×10^{-3}	120.9	3.51	8.91×10^{-3}
cyclic-PAzoMA ₁₂		5630	1.15	56.1	74.3	2.19	6.30×10^{-3}	106.4	1.87	4.93×10^{-3}
linear-PAzoMA ₁₈	7130	9170	1.18	76.4	89.2	5.47	1.50×10^{-2}	129.0	5.02	1.25×10^{-2}
cyclic-PAzoMA ₁₈		8250	1.16	57.6	74.5	2.66	7.65×10^{-3}	105.9	1.49	3.93×10^{-3}
linear-PAzoMA ₃₅	13860	14000	1.10	78.9	91.3	2.92	8.01×10^{-3}	131.3	2.50	6.18×10^{-3}
cyclic-PAzoMA ₃₅		12160	1.09	60.3	85.9	2.27	6.32×10^{-3}	120.2	1.68	4.27×10^{-3}

^a \overline{M}_n : number-average molecular weight; PDI: polydispersity index; T_g : glass transition temperature; T_{sn} , ΔH_{sn} , and ΔS_{sn} : smectic-to-nematic phase transition temperature, enthalpy, and entropy, respectively; T_{ni} , ΔH_{ni} , and ΔS_{ni} : nematic-to-isotropic phase transition temperature, enthalpy, and entropy, respectively. ^b From ¹H NMR spectra. ^c From SEC measurements

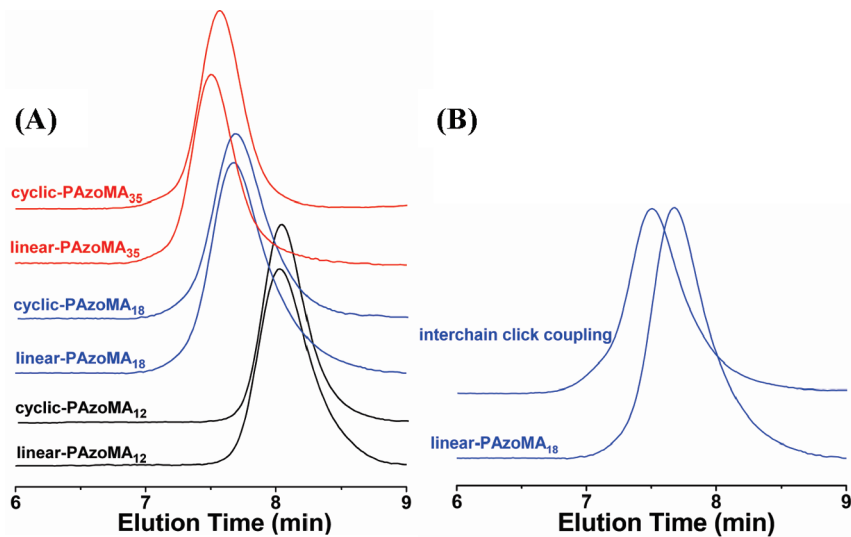


Figure 1. Size-exclusion chromatograph curves: (A) linear- and cyclic azobenzene-containing side-chain liquid crystalline polymers of different molecular weights; (B) linear precursor and the sample obtained by reaction at a high precursor concentration (about 100 times the concentration used for cyclization) showing interchain coupling.

in the polarization variation of a probe light. A weak He–Ne laser (633 nm, 4 mW) was used to provide the probe beam at normal incidence, having little effect on the isomerization of azobenzene mesogens. With the crossed polarizers, the polarization change of the probe light led to a transmission intensity variation measured by means of a photodetector, which allowed the photoinduced birefringence to be calculated. In a typical experiment, when the photoinduced birefringence reached stabilization state (under the linearly polarized excitation), the excitation beam was turned off for a period of time for the observation of its stability in time. This was followed by the application of a circularly polarized excitation beam of the Ar⁺ ion laser (obtained by means of adding a quarter-wave plate on the optical path of the same excitation beam), and the dynamic process of erasure of the orientation axes of azobenzene mesogens in the film plane was also recorded.

On the other hand, thin polymer films (thickness ~40 nm) were prepared on a quartz plate, for which the photoinduced orientation of azobenzene mesogens at room temperature and the effect of thermal annealing into the LC phases could be characterized by using an order parameter calculated from the linear dichroism of the absorption band of *trans*-azobenzene at around 360 nm. In this experiment, all films were also pre-irradiated with a UV light ($\lambda = 360$ nm, 10 mW cm⁻², 1 min) at room temperature before being exposed to linearly polarized visible light ($\lambda = 440$ nm, 1.4 mW cm⁻², 30 min). The used UV and visible light were obtained by using a spot curing system (Novacure 2100) combined with interference filters (10 nm bandwidth, Oriel). The films were then annealed in an oven with a preset temperature for 10 min before being taken off from the oven for polarized UV-vis measurements at room temperature.

Results and Discussion

1. Synthesis of Cyclic Side-Chain Liquid Crystalline Polymers. Three samples of different molecular weights of linear-PAzoMA, with a terminal alkyne and an azide group, were synthesized using ATRP followed by a chain-end functionalization reaction (Scheme 1). M_n of these linear polymer precursors were determined from their ¹H NMR spectra (see below) and also from SEC using PS standards. The results are given in Table 1; the number in the acronym of each sample is the number of monomer units calculated from the NMR-based M_n . Under the used conditions, in particular the high dilution of linear polymer precursor ensured by its very slow addition into the reaction solution, the intrachain click reaction of the alkyne and azide end groups of the linear-PAzoMA precursors resulted in their cyclization, giving rise to cyclic-PAzoMA. The successful cyclization, rather than condensation, was revealed by the results obtained using a number of characterization methods. Figure 1a shows the SEC curves of all three cyclic polymers and their linear counterparts. In all cases, the cyclic polymer displayed a longer retention time (larger retention volume) than the linear counterpart, meaning that the cyclic polymer has a smaller hydrodynamic volume than the linear one. The difference in retention time is most prominent between the samples with the largest size (linear- and cyclic-PAzoMA₃₅) while it is less important for the samples with a lower M_n , which is consistent with reports on conventional polymers. Without ruling out the possibility of having traces of linear species in the cyclic samples, the display of longer retention times, together with the spectral evidence of an effective click

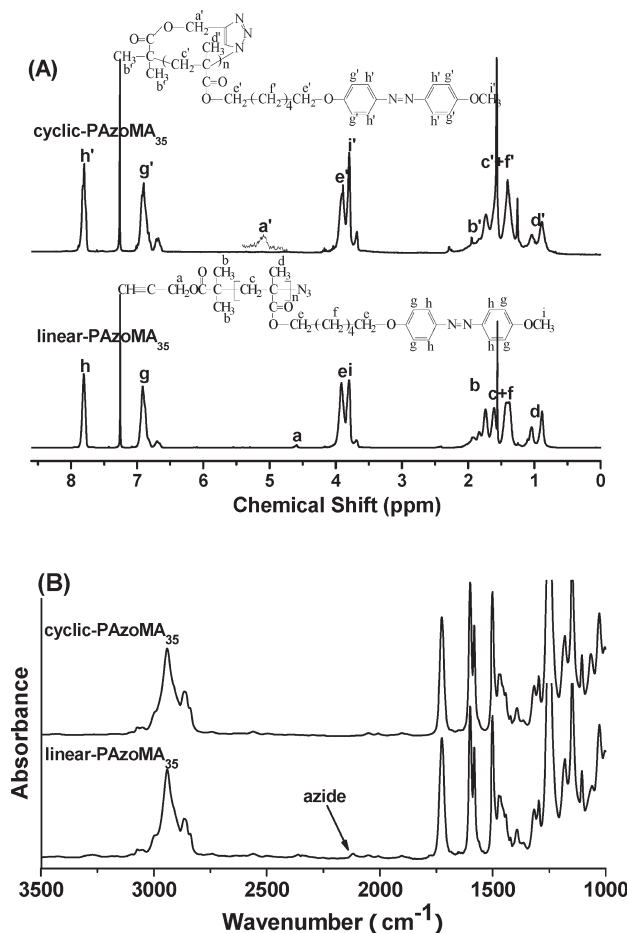


Figure 2. (A) ¹H NMR and (B) infrared spectra of linear- and cyclic-PAzoMA₃₅.

reaction between alkyne and azide groups (see below), clearly indicates the absence of any meaningful amount of linear polymers. The apparent changes in molecular weight from the SEC measurements are shown in Table 1. We also conducted a control test to observe the difference between cyclization (intrachain coupling) under the high dilution condition and condensation (interchain coupling) at a high concentration of the polymer precursor. Figure 1b compares the SEC curves of linear-PAzoMA₁₈ and the sample obtained after 15 h of reaction at a precursor concentration about 100 times that used for preparing the cyclic polymers in Figure 1a (all other conditions were kept the same). In this case, the sample displayed shorter retention times than the linear precursor, indicating the formation of species with an increased molecular weight that could only be formed by interchain coupling. The apparent M_n increased from 9170 to 14 750 and the PDI from 1.18 to 1.28.

¹H NMR and infrared spectroscopic measurements also confirmed the occurrence of the cycloaddition reaction between the alkyne and azide groups. Figure 2 shows the ¹H NMR and IR spectra of linear- and cyclic-PAzoMA₃₅ as example. From NMR, on the one hand, the methylene protons next to the alkyne group had a signal at ~4.6 ppm. (This peak was used to determine M_n of the linear polymer through comparison of integrals.) This characteristic signal disappeared for the cyclic polymer which displayed a new signal (weak but noticeable) at ~5.2 ppm, attributed to methylene protons next to 1,2,3-triazole.^{3,6} From IR, on the other hand, it is seen that the characteristic absorption band of azide groups at ~2110 cm⁻¹ of the linear polymer was absent

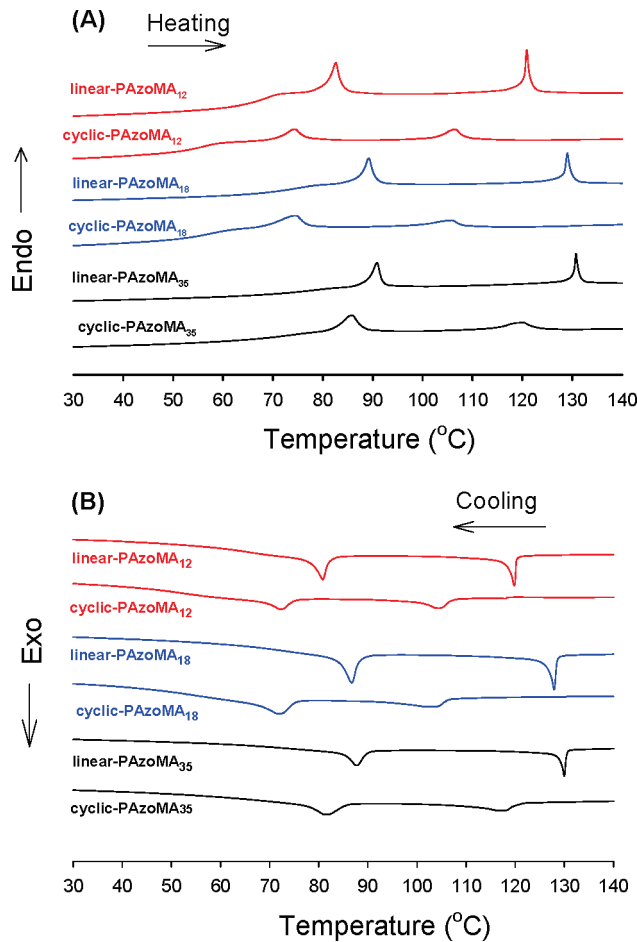


Figure 3. DSC heating (A) and cooling (B) curves of linear- and cyclic azobenzene-containing side-chain liquid crystalline polymers of different molecular weights (second scan).

for the cyclic polymer. All the results indicate that the “click” cyclization of α -alkynyl- ω -azido heterodifunctional linear polymers under high dilution is an efficient way to prepare cyclic azobenzene-containing SCLCPs.

2. Thermal Mesophase Transitions. As compared to linear SCLCP, the topological constraint subjected by cyclic SCLCP would understandably influence the order and organization of the side-group mesogens. This was indeed observed from changes in mesophase transition temperature, enthalpy, and entropy. Figure 3 show the DSC heating and cooling curves (second scan) of the three linear- and cyclic-PAzoMA; the different thermal behaviors are evident. The used linear SCLCP is known to display a nematic and smectic-A phase;¹⁹ on heating to and cooling from the isotropic phase, the phase transition endotherms (peaked at T_{sn} and T_{ni}) and exotherms (T_{in} and T_{ns}), respectively, are visible. For the cyclic SCLCP, the two mesophase transitions remained but occurred at significantly lower temperatures and with broadened transition endothermic or exothermic peaks. The smectic-to-nematic and nematic-to-isotropic phase transition temperatures on heating (T_{sn} and T_{ni}) as well as the corresponding enthalpies (ΔH_{sn} and ΔH_{ni}) and entropies (ΔS_{sn} and, ΔS_{ni}), calculated according to $\Delta S_{sn(or ni)} = \Delta H_{sn(or ni)}/T_{sn(or ni)}$, are also summarized in Table 1. And to better illustrate the effect of molecular weight on the differences between linear- and cyclic-PAzoMA, their T_g and two mesophase transition temperatures measured on the heating scan are plotted as a function of M_n (NMR) in Figure 4. It can be seen that all cyclic polymers have lower T_g and LC phase transition temperatures

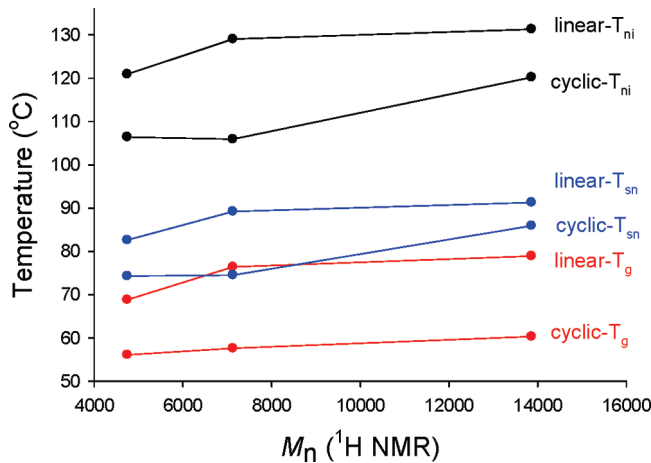


Figure 4. Glass and mesophase transition temperatures (on heating) vs molecular weight for linear- and cyclic azobenzene-containing side-chain liquid crystalline polymers.

than their linear counterparts. With respect to cyclic-PAzoMA₃₅, the decreases appear to be more important for the two cyclic polymers of smaller sizes, revealing a greater topological constraint effect on smaller cycles of SCLCP. However, cyclic-PAzoMA₁₈ and cyclic-PAzoMA₁₂ displayed similar mesophase transition temperatures. From Table 1, it can also be noticed that the topological constraint effect in cyclic-PAzoMA led to a reduction of the mesophase transition enthalpy and entropy. Qualitatively, the smaller phase transition enthalpies suggest a decreased molecular order of mesogens in the LC phases of cyclic polymers, weakening the intermolecular interactions. As for the smaller phase transition entropies, this may be accounted by a more important reduction of polymer chain mobility in the isotropic phase with respect to the nematic phase (for ΔS_{ni}) and in the nematic phase with respect to the smectic phase (for ΔS_{sn}). We carried out powder X-ray diffraction measurements on linear- and cyclic-PAzoMA, but the results did not show any noticeable difference on the ordering of smectic layers, noting that even for linear-PAzoMA, smectic layers were difficult to develop to be observed by X-ray diffraction.

Figure 5 shows an example of polarizing optical micrographs with linear- and cyclic-PAzoMA₃₅. They were taken in the course of cooling from the isotropic phase, at two temperatures in the nematic and smectic phase, respectively. Knowing that the smectic layers were difficult to develop in these polymers, the micrographs in the smectic phase were recorded after 24 h of annealing at the chosen temperature (84 °C for linear-PAzoMA₃₅ and 77 °C for cyclic-PAzoMA₃₅). For both samples, the transition from nematic to smectic phase resulted in a change in the LC texture; however, despite the thermal treatment, no clear focal conic texture could be observed for the smectic phase, and the samples showed mainly a schlieren texture of nematic phase. The difference between the linear and cyclic polymer is clear, particularly in the nematic phase, where the cyclic sample displayed more threads under crossed polarizers, indicating more and smaller nematic domains with changing LC directors. This may also be a manifestation of the topological constraint effect that hampers the LC order and causes more defects in the cyclic SCLCP.

3. Photoinduced Anisotropy. The use of SCLCP bearing azo mesogens also made it possible to investigate the effect of topological constraint arising from chain cyclization on the photoinduced anisotropy as a result of the trans–cis isomerization of the chromophore, which is a major interest for azo polymers.^{20–28} Two types of experiments were performed.

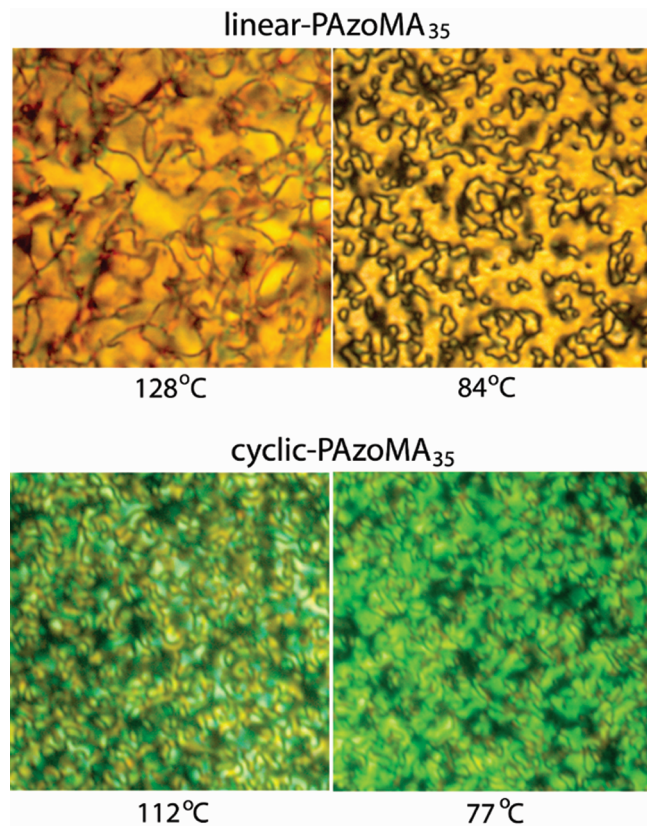


Figure 5. Polarizing optical micrographs of linear- and cyclic-PAzoMA₃₅ recorded, upon cooling from isotropic phase, at two temperatures in the nematic and smectic phase, respectively. Image area: 67 $\mu\text{m} \times 67 \mu\text{m}$.

On the one hand, the kinetics of photoinduced birefringence in thick polymer films (thickness $\sim 10 \mu\text{m}$) at room temperature was monitored upon excitation at 488 nm using an Ar ion laser.¹⁸ On the other hand, the development of photo-induced orientation of azo mesogens in thin films (thickness $\sim 40 \text{ nm}$) upon annealing in the LC phases was measured by recording polarized UV–vis spectra. In both experiments, prior to the excitation using a linearly polarized visible light, all films were preirradiated with an unpolarized UV lamp to obtain the photostationary cis-rich state for azo mesogens, which is a known treatment for azo SCLCP whose *trans*-azobenzene absorbs at around 360 nm.^{23,27,28} Before reporting and discussing the results, we mention that the UV–vis absorption spectra of linear- and cyclic-PAzoMA are quite similar, and the trans–cis photoisomerization occurs both in solution and in the solid state. An example of the UV–vis spectra of thin films of linear- and cyclic-PAzoMA₃₅ is shown in Figure 6. The two films were cooled from isotropic phase to room temperature before recording the spectra. Prior to UV irradiation, the same spectral shapes indicate a similar aggregation state of azo mesogens in the linear and cyclic polymer, displaying a broad absorption band peaked at about 360 nm ($\pi-\pi^*$ transition of nonaggregated trans azo) with blue-shifted (H-aggregation) and red-shifted (J-aggregation) shoulders. In both cases, the photostationary cis-reach state could readily be obtained after 1 min UV irradiation (360 nm, 10 mW cm⁻²) inducing the trans–cis isomerization. From the decrease of absorption of the trans isomer, being accompanied by the increase of absorption of cis isomer peaked at $\sim 450 \text{ nm}$ ($n-\pi^*$ transition), the population of cis-azo mesogens is about 77% for the linear polymer and 72% for the cyclic polymer. From this photostationary

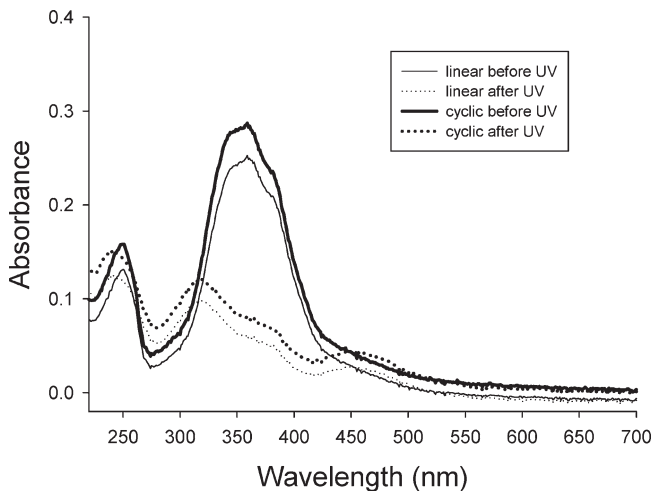


Figure 6. UV-vis spectra of thin films of linear- and cyclic-PAzoMA₃₅ recorded at room temperature before and after an UV irradiation (360 nm, 10 mW cm⁻², 1 min), leading to the photostationary state that is rich in *cis*-azobenzene.

state, excitation with a linearly polarized visible light (usually > 440 nm) can bring azo mesogens in the *cis* form back to the trans form, with concomitant orientation of azo mesogens perpendicularly to the polarization of the visible light.

The kinetics of photoinduced birefringence at room temperature for linear and cyclic polymers of two different sizes, PAzoMA₃₅ and PAzoMA₁₈, are compared in Figure 7. A typical experiment consisted in first applying a linearly polarized 488 nm light to induce the birefringence, then turning off the excitation to examine the stability of the birefringence, and finally applying a circularly polarized light to “erase” the “in-plane” anisotropy.²⁹ For all films, the small birefringence existing prior to the linearly polarized excitation was normalized to zero to better show the part of the photoinduced birefringence. From the results, it becomes immediately clear that the cyclic polymers behave differently from their linear precursors. For the two polymer sizes investigated, upon the laser excitation, the photoinduced birefringence in the linear polymers grows monotonically and reaches a greater value than in the cyclic polymers. This indicates that the greater topological constraint in cyclic polymers makes the orientation of azo mesogens more difficult to develop. More interestingly, the dynamic processes are also very different. For the two linear polymers, they have a similar two-process anisotropy increase and erasure, with PAzoMA₁₈ exhibiting faster times and higher birefringence than PAzoMA₃₅, likely due to an effect of polymer size. For both birefringence induction upon linearly polarized excitation and its subsequent erasure by circularly polarized light, the signal changes are quite monotonic over time, and the fast and slow processes can be well fitted with two exponentials, giving rise to their rate ratio and signal ratio (relative contribution to the anisotropy). For linear-PAzoMA₃₅, these two ratios are 5.7 and 1.6 for birefringence induction and 5.7 and 1.3 for its erasure, while with linear-PAzoMA₁₈, they are 6.0 and 1.3 for birefringence induction and 8.5 and 1.0 for erasure (curve fittings not shown in the figure for the sake of clarity).

By contrast, the cyclic polymers display more complicated dynamic processes, and the signal changes appear nonmonotonic. In the case of cyclic-PAzoMA₃₅, upon linearly polarized excitation, there is a fast increase in birefringence, and then it is decreased before increasing again more slowly; after about 140 s of excitation, the increase rate is further slowed

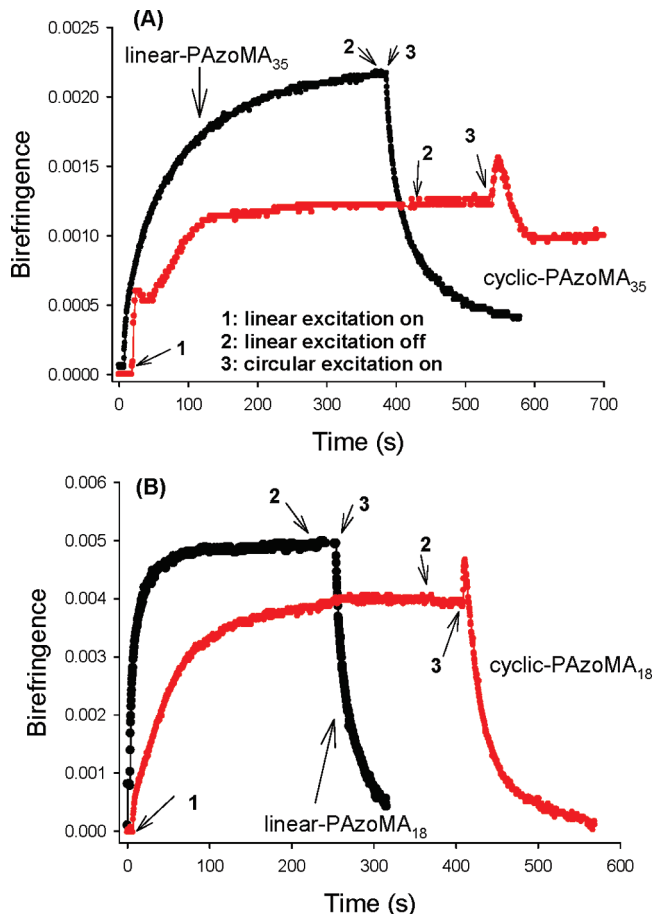


Figure 7. Dynamic processes of photoinduced birefringence of (A) linear- and cyclic-PAzoMA₃₅ and (B) linear- and cyclic-PAzoMA₁₈. The turn-on and turn-off times of the linearly polarized excitation light as well as the turn time of the circularly polarized light are indicated by arrows.

down before the final stabilization of the signal. More strikingly, when exposed to circularly polarized light, there is a fast transient increase of the apparent birefringence (increase in transmission of the probe light under crossed polarizers), followed by a partial decrease of the birefringence. Such nonmonotonic behaviors are also visible for the smaller cyclic-PAzoMA₁₈. The nonmonotonic increase in birefringence suggests that there may be at least two mechanisms that are acting in opposite directions during linearly polarized excitation, while the fast increase in transmission upon circularly polarized excitation suggests the occurrence of transient out-of-plane reorientation of azo mesogens.³⁰ Although the exact mechanisms accounting for the peculiar behaviors of cyclic polymers are unclear at this time, the fact that these are observed only after cyclization point to an origin of topological constraints.

Another experimental design also confirmed the topological constraint effect on the photoinduced anisotropy in cyclic azo SCLCPs. Thin films were prepared on quartz plates to exhibit an absorbance at 360 nm suitable for measuring the orientation of trans azo mesogens. They were preirradiated at room temperature with unpolarized UV light to reach the photostationary *cis*-rich state (this should also create an anisotropy axis perpendicular to the film plane since the light was normally incident)²⁹ and then exposed to linearly polarized visible light to induce an “in-plane” orientation of trans azo mesogens in the direction perpendicular to the polarization of the excitation visible light. This photoinduced molecular orientation in thin films could be

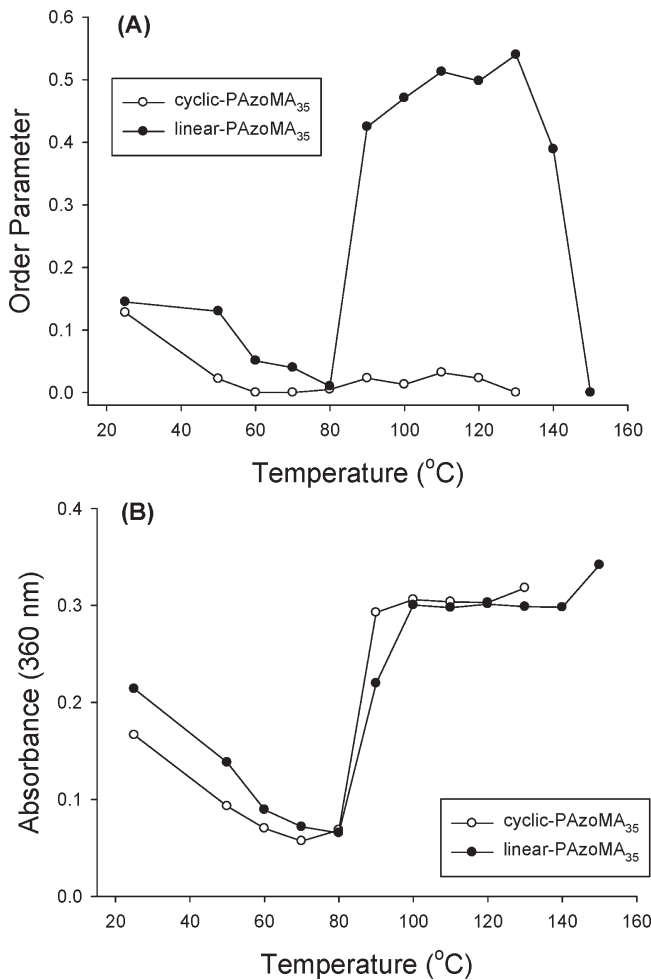


Figure 8. Plots of (A) order parameter vs temperature and (B) absorbance at 360 nm vs temperature for linear- and cyclic-PAzoMA₃₅.

measured by recording polarized UV-vis spectra with the polarization of the spectrophotometer's beam set to be parallel (A_{\parallel}) and perpendicular (A_{\perp}) to the polarization of the excitation visible light; from the dichroic ratio of the 360 nm band ($R = A_{\perp}/A_{\parallel}$) the order parameter S , characterizing the average orientation of trans azo mesogens, could be calculated according to $S = (R - 1)/(R + 2)$. A well-known property of azo SCLCPs is that when such a film is heated to above T_g of the polymer and annealed in a LC phase, the chain mobility allows mesogenic side groups to better organize, and during this process, the initial photoinduced orientation of azo mesogens could serve as seed and lead to a much enhanced orientation of the mesogens.^{20–28} We carried out the experiments with the two cyclic polymers and their linear precursors. The results are summarized in Figure 8 for linear- and cyclic-PAzoMA₃₅ and in Figure 9 for linear- and cyclic-PAzoMA₁₈. Figures 8a and 9a are plots of order parameter as a function of annealing temperature (10 min at each temperature before cooling to room temperature for the measurements), while Figures 8b and 9b are plots of absorbance of the 360 nm band (calculated from $(A_{\parallel} + 2A_{\perp})/3$) vs temperature. Similar observations can be made for the two sizes of polymers, and the same conclusions can be reached.

With the used thin films, all samples had a similar photoinduced orientation of azo mesogens initially. As the films were annealed at $T > T_g$, over a temperature range in the smectic A phase (about 60–80 °C), they all showed a decrease of the order parameter. This apparently surprising

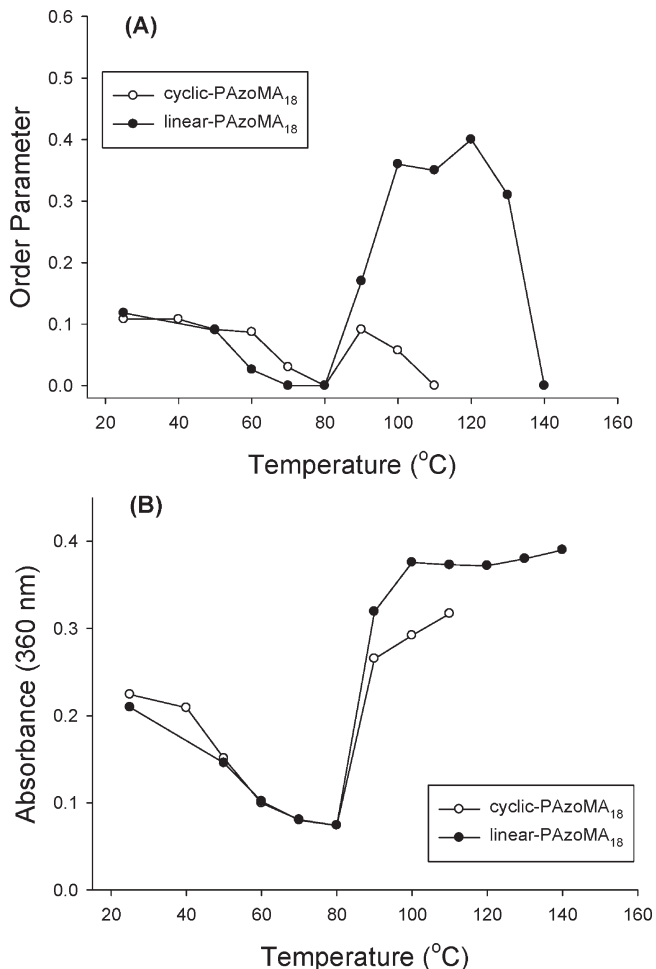


Figure 9. Plots of (A) order parameter vs temperature and (B) absorbance at 360 nm vs temperature for linear- and cyclic-PAzoMA₁₈.

behavior can be explained from the change in absorbance of the 360 nm band. The drop of order parameter coincides with a drop of the absorbance, which indicates that the reorganization of azo mesogens in the smectic phase resulted in a homeotropic alignment. It appears that in the thin films, for which the interaction of polymers with the substrate surface would be important, smectic layers with azo mesogens preferentially aligned perpendicular to the film surface are energetically more stable. In this temperature range, the difference between cyclic and linear polymers, if there was any, could not be assessed within experimental error (about 20% on the value of order parameter) due to the low orientation degree. When the films were further annealed at higher temperatures, into the nematic phase, the mesophase transition turn azo mesogens to lie in the film plane, as can be seen from the recovered absorbance in all samples. In the nematic phase, the orientation of azo mesogens in the two linear polymers was much enhanced as revealed by the risen order parameter (error <10%). In this case, the initial photoinduced orientation of azo mesogens served as a template to amplify the macroscopic orientation, leading to a monodomain in the nematic phase. By sharp contrast, with the two cyclic polymers, this photoinduced orientation could not develop in the nematic phase; the small order parameter indicates a polydomain morphology in the nematic phase, revealing again the topological constraint effect that hinders the ordering and organization of mesogenic side groups. In all cases, when heated to the isotropic phase, the orientation of azo mesogens was erased.

Conclusions

A cyclic SCLCP bearing azobenzene mesogens was synthesized, characterized, and studied for the first time. We showed that the “click” cyclization of α -alkynyl- ω -azido heterodifunctional linear SCLCPs under high dilution is an effective way to synthesize cyclic SCLCPs. The ring structure-imposed topological constraint effect on LC phase transitions (temperature, enthalpy, and entropy), LC order, and the photoinduced orientation of azobenzene mesogens was evidenced by comparing the behaviors of cyclic-PAzoMA with the linear polymer precursor. Cyclic polymers exhibited a lower T_g , T_{sn} , and T_{ni} as well as smaller phase transition enthalpy and entropy than the linear polymer counterparts, the differences being more important for smaller ring sizes. As for the photoinduced birefringence, it was smaller in the cyclic polymers than in the linear polymers, and the dynamic processes of birefringence induction and erasure upon linearly and circularly polarized excitation, respectively, were very different as well. While linear-PAzoMA showed monotonic changes over time, cyclic-PAzoMA displayed nonmonotonic changes. Moreover, for cyclic-PAzoMA, the photoinduced orientation of azobenzene mesogens inscribed at room temperature could not be enhanced by subsequent annealing in the nematic phase, contrary to the linear polymers. All these results indicate that the topological constraint in cyclic SCLCPs affects profoundly the arrangement and organization of mesogenic side groups as well as their orientation processes in response to an external stimulus such as light. This finding points out that chain cyclization of linear SCLCPs is a way to change the coupling of mesogenic side groups with chain backbone; the interplay of the two constituents under the additional topological constraint may be explored to generate new properties or functions. More studies are underway in our laboratory, and the results will be published at due time.

Acknowledgment. We acknowledge the financial support from the Natural Sciences and Engineering Research Council of Canada (NSERC) and le Fonds québécois de la recherche sur la nature et les technologies of Québec (FQRNT). Y.Z. is a member of the FQRNT-funded Center for Self-Assembled Chemical Structures.

References and Notes

- (1) Semlyen, J. A. *Cyclic Polymers*, 2nd ed.; Kluwer Academic: Dordrecht, The Netherlands, 2000.

- (2) Kricheldorf, H. R. *J. Polym. Sci., Part A: Polym. Chem.* **2010**, *48*, 251–284.
- (3) Laurent, B. A.; Grayson, S. M. *Chem. Soc. Rev.* **2009**, *38*, 2202–2213.
- (4) Bielawski, C. W.; Benitez, D.; Grubbs, R. H. *Science* **2002**, *297*, 2041–2044.
- (5) Schappacher, M.; Deffieux, A. *Science* **2008**, *319*, 1512–1515.
- (6) Laurent, B. A.; Grayson, S. M. *J. Am. Chem. Soc.* **2006**, *128*, 4238–4239.
- (7) Xu, J.; Ye, J.; Liu, S. *Macromolecules* **2007**, *40*, 9103–9110.
- (8) Eugene, D. M.; Grayson, S. M. *Macromolecules* **2008**, *41*, 5082–5084.
- (9) Hoskins, J. N.; Grayson, S. M. *Macromolecules* **2009**, *42*, 6406–6413.
- (10) Hu, J.; Zheng, R.; Wang, J.; Hong, L.; Liu, G. *Macromolecules* **2009**, *42*, 4638–4645.
- (11) Dong, Y.-Q.; Tong, Y.-Y.; Dong, B.-T.; Du, F.-S.; Li, Z.-C. *Macromolecules* **2009**, *42*, 2940–2948.
- (12) Beauchage, G.; Kulkarni, A. S. *Macromolecules* **2010**, *43*, 532–537.
- (13) Santangelo, P. G.; Roland, C. M.; Chang, T.; Cho, D.; Roovers, J. *Macromolecules* **2001**, *34*, 9002–9005.
- (14) Viras, K.; Yan, Z.-G.; Price, C.; Booth, C.; Ryan, A. J. *Macromolecules* **1995**, *28*, 104–109.
- (15) Percec, V.; Kawasumi, M. *Macromolecules* **1992**, *25*, 3851–3861.
- (16) Percec, V.; Asandei, A. D.; Chu, P. *Macromolecules* **1996**, *29*, 3736–3750.
- (17) Ringsdorf, H.; Schmidt, H. W. *Makromol. Chem.* **1984**, *185*, 1327–1334.
- (18) (a) Zhao, Y.; Bai, B.; Asatryan, K.; Galstian, T. *Adv. Funct. Mater.* **2003**, *13*, 781–788. (b) Cui, L.; Zhao, Y.; Yavrian, A.; Galstian, T. *Macromolecules* **2003**, *36*, 8246–8252.
- (19) Walther, M.; Faulhammer, H.; Finkelman, H. *Macromol. Chem. Phys.* **1998**, *199*, 223–237.
- (20) Ichimura, K. *Chem. Rev.* **2000**, *100*, 1847–1873.
- (21) Natansohn, A.; Rochon, P. *Chem. Rev.* **2002**, *102*, 4139–4175.
- (22) (a) Ikeda, T. *J. Mater. Chem.* **2003**, *13*, 2037–2057. (b) Yu, H.; Naka, Y.; Shishido, A.; Ikeda, T. *Macromolecules* **2008**, *41*, 7959–7966. (c) Yu, H.; Shishido, A.; Li, J.; Kamata, K.; Iyoda, T.; Ikeda, T. *J. Mater. Chem.* **2007**, *17*, 3485–3488.
- (23) (a) Seki, T. *Bull. Chem. Soc.* **2007**, *80*, 2084–2109. (b) Uekusa, T.; Nagano, S.; Seki, T. *Macromolecules* **2009**, *42*, 312–318.
- (24) Wang, D.; Ren, H.; Wang, X.; Wang, X. *Macromolecules* **2008**, *41*, 9382–9388.
- (25) Yager, K. G.; Barrett, C. J. *Curr. Opin. Solid State Mater. Sci.* **2001**, *5*, 487–494.
- (26) Zhao, Y.; Ikeda, T., Eds.; *Smart Light-Responsive Materials: Azobenzene-Containing Polymers and Liquid Crystals*; John Wiley: Hoboken, NJ, 2009.
- (27) Wu, Y.; Zhang, Q.; Kanazawa, A.; Shiono, T.; Ikeda, T.; Nagase, Y. *Macromolecules* **1999**, *32*, 3951–3956.
- (28) Tong, X.; Cui, L.; Zhao, Y. *Macromolecules* **2004**, *37*, 3101–3112.
- (29) Yavrian, A.; Galstian, T.; Piche, M. *Opt. Eng.* **2002**, *41*, 852–855.
- (30) Saad, B.; Galstyan, T.; Denariez-Roberge, M. M.; Dumont, M. *Opt. Commun.* **1998**, *151*, 235–240.